



# Formation and maintenance of high-nitrate, low pH layers in the eastern Indian Ocean and the role of nitrogen fixation

A. M. Waite<sup>1</sup>, V. Rossi<sup>2</sup>, M. Roughan<sup>2</sup>, B. Tilbrook<sup>3</sup>, P. A. Thompson<sup>4</sup>, M. Feng<sup>5</sup>, A. S. J. Wyatt<sup>6</sup>, and E. J. Raes<sup>1</sup>

<sup>1</sup>The Oceans Institute and School of Environmental Systems Engineering, M047 University of Western Australia, Crawley, WA 6009, Australia

<sup>2</sup>School of Mathematics and Statistics, University of New South Wales, Sydney, NSW 2052, Australia

<sup>3</sup>CSIRO Wealth from Oceans National Research Flagship and Antarctic Climate and Ecosystems CRC, Hobart, Tasmania 7001, Australia

<sup>4</sup>CSIRO Wealth from Oceans National Research Flagship, Hobart, Tasmania 7001, Australia

<sup>5</sup>CSIRO Wealth from Oceans National Research Flagship, Underwood Avenue, Floreat, WA 6014, Australia

<sup>6</sup>Marine Biogeochemistry Laboratory, Department of Chemical Oceanography, Atmosphere and Ocean Research Institute, The University of Tokyo, Kashiwa, Chiba, 277-8564, Japan

Correspondence to: A. M. Waite (anya.waite@uwa.edu.au)

Received: 14 January 2013 – Published in Biogeosciences Discuss.: 1 March 2013

Revised: 21 June 2013 – Accepted: 10 July 2013 – Published: 28 August 2013

**Abstract.** We investigated the biogeochemistry of low dissolved oxygen high-nitrate (LDOHN) layers forming against the backdrop of several interleaving regional water masses in the eastern Indian Ocean, off northwest Australia adjacent to Ningaloo Reef. These water masses, including the forming Leeuwin Current, have been shown directly to impact the ecological function of Ningaloo Reef and other iconic coastal habitats downstream. Our results indicate that LDOHN layers are formed from multiple subduction events of the Eastern Gyral Current beneath the Leeuwin Current (LC); the LC originates from both the Indonesian Throughflow and tropical Indian Ocean. Density differences of up to  $0.025 \text{ kg m}^{-3}$  between the Eastern Gyral Current and the Leeuwin Current produce sharp gradients that can trap high concentrations of particles (measured as low transmission) along the density interfaces. The oxidation of the trapped particulate matter results in local depletion of dissolved oxygen and regeneration of dissolved nitrate (nitrification). We document an associated increase in total dissolved carbon dioxide, which lowers the seawater pH by 0.04 units. Based on isotopic measurements ( $\delta^{15}\text{N}$  and  $\delta^{18}\text{O}$ ) of dissolved nitrate, we determine that  $\sim 40$ – $100\%$  of the nitrate found in LDOHN layers is likely to originate from nitrogen fixation, and that, regionally, the importance of N-fixation in contributing to LDOHN layers is likely to be highest at the surface and offshore.

## 1 Introduction

Nitrogen (N) sources entering the surface ocean via nitrogen fixation are in some cases the dominant source of bioavailable N supporting primary production (Codispoti, 2007; Gruber, 2011). This fixation of N is biologically linked to simultaneous fixation of carbon (C) into planktonic biomass, which may sink to the deep sea (Siegenthaler and Sarmiento, 1993). The relative importance of turbulent fluxes of N into the surface ocean across the pycnocline as new nitrate, the fluxes entering the surface ocean through N-fixation, and their influence on carbon dioxide uptake in the eastern Indian Ocean (IO) are all poorly understood. Takahashi et al. (2009) estimated a net air–sea flux of carbon dioxide ( $\text{CO}_2$ ) into the ocean of  $2 \times 10^{15} \text{ g}$  (2 Pg) per year using a surface  $\text{CO}_2$  climatology normalized to the year 2000. The climatology indicates many of the subtropical waters of the South Indian Ocean are a  $\text{CO}_2$  sink, although there is little surface  $\text{CO}_2$  data available from the region to assess the seasonal through inter-annual changes in the air–sea flux of carbon. Valsala et al. (2012) utilized a biogeochemical model to indicate that much of the variability of the air–sea  $\text{CO}_2$  flux for the subtropical region was driven by changes in the solubility pump. However, the importance of the biological pump in these processes remains largely unexamined.

In the eastern IO off Western Australia, Thompson et al. (2011) documented the presence of a subsurface layer of relatively low dissolved oxygen and high nitrate (LDOHN) immediately beneath the poleward-flowing Leeuwin Current, a boundary current off Western Australia. More recently, we measured multiple subsurface ( $\sim 100$ – $250$  m) LDOHN layers during austral autumn 2010 (Rossi et al., 2013). These subsurface layers had distinct and variable temperature and salinity signatures, possibly indicating they originated in different water masses. Rossi et al. (2013) attributed variations of subsurface nitrate within these layers to local in situ remineralization of organic matter that accumulated on sharp physical interfaces and also speculated this might be favoured by the proximity of oxygenated subsurface waters. We thus illuminated the presence of a shallow source of dissolved nitrate likely to have been derived from the oxidation of particulate matter, and regenerated relatively close to the surface, which could influence local  $\text{CO}_2$  concentrations and air–sea  $\text{CO}_2$  fluxes. However, the precise sources and processes contributing to the nitrogen, oxygen and particles within this layer remain unclear. Identifying the sources of particulate organic matter, N and O contributing to this layer is critical for our understanding of the regional sources and sinks of both nitrogen and the associated carbon flux.

Here we investigate particle sources and nitrate dynamics in the formation region of the Leeuwin Current between  $21$  and  $23^\circ$  S. We analyse continuous vertical nitrate measurements, and utilize the nitrogen and oxygen isotopic signature of dissolved nitrate ( $\delta^{15}\text{N}$  and  $\delta^{18}\text{O}$ ), to distinguish the sources of the nitrate between upward fluxes of subsurface N as new nitrate and a flux due to nitrogen fixation. We link shallow regeneration of nitrate in the LDOHN layers with their impact on the carbonate system. Our data showed that  $\text{TCO}_2$  generation by organic matter remineralization caused a lowering of pH and a decrease in dissolved oxygen concentrations in the subsurface LDOHN layers.

## 2 Materials and methods

### 2.1 Primary research voyage

We sampled coastal waters from the  $50$  m to the  $1000$  m isobaths, along seven transects from  $21$  to  $23^\circ$  S off north-west Australia from 10 to 22 May 2010. Here, the Leeuwin Current consolidates from several surface pathways, including warm and saline waters coming from the Indonesian Throughflow (Western Pacific) and the tropical Indian Ocean, fresher Indonesian waters transported by the Eastern Gyral Current (EGC) (Domingues et al., 2007), and cooler, more saline waters from the South Indian Ocean (Figs. 1 and 2a–e). Conductivity, temperature, and depth (CTD) measurements were made using a rosette system that carried a Wet-labs C-Star<sup>TM</sup> transmissometer, a Seabird dissolved oxygen sensor (SBE43) and a Satlantic ISUS<sup>TM</sup> sensor. Transmission

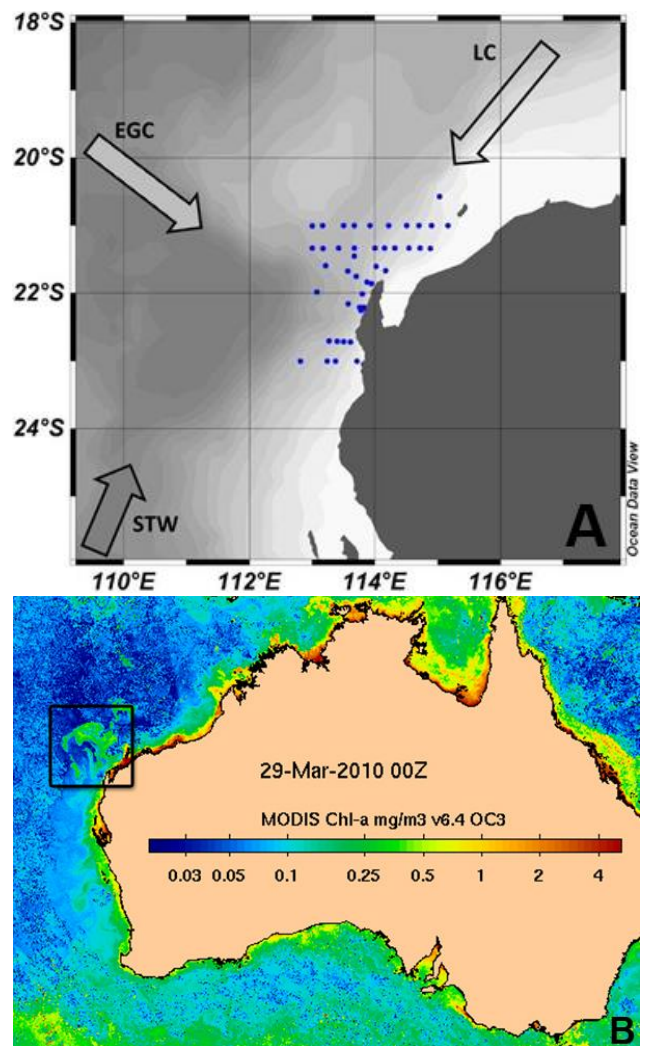


**Fig. 1.** (A) Map of study area showing sampling locations as filled circles and the direction of inflow of the major regional water masses and currents: the Leeuwin Current (LC) waters sourced variously from the Indonesian Throughflow (ITF) and from tropical waters (see Domingues et al., 2007); the Eastern Gyral Current (EGC) sourced from fresher, cooler tropical waters; and the subtropical water (STW) from the open Indian Ocean, which are saline and relatively cold. (B) Modis ocean colour image from 30 March 2010 produced by IMOS, showing large ( $100\text{ km} \times 100\text{ km}$ ) bloom northwest of the study area, which was transected early in April 2010 and observed to be a surface bloom of *Trichodesmium* sp.

was used as an indicator of particle concentration (Karageorgis et al., 2008). Chlorophyll *a* (Parsons et al., 1984), total alkalinity and total dissolved inorganic carbon (DIC) measurements were made on samples from bottles fired at up to 10 depths, with 3–4 samples identified as being specifically within or outside the LDOHN layer. Total dissolved inorganic carbon dioxide ( $\text{TCO}_2$ ) was analysed following the colorimetric procedure (Johnson et al., 1993; Takahashi et al., 2009; Dickson, 2007). Total alkalinity was analysed

using an open cell potentiometric titration of a 100 mL sample with 0.1 N HCl after Dickson et al. (2007). The accuracy and precision of the  $TCO_2$  and total alkalinity measurements was verified as  $\pm 2 \mu\text{mol L}^{-1}$  based on analyses of certified reference seawater samples from Scripps Institute of Oceanography. pH was calculated using the Ocean Data View software, which uses an iterative Newton method, with constants following Dickson (2007). Dissolved inorganic nitrate (nitrate and nitrite, hereafter nitrate) was analysed for all depths using QuickChem™ methods on a flow injection LACHAT® instrument as per the following protocols for nitrate + nitrite (QuikChem™ Method 31-107-04-1-A; detection limit  $\sim 0.03 \mu\text{mol L}^{-1}$ ; adapted from Wood et al., 1967). For calibration of the ISUS sensor, up-cast nitrate profiles derived from in situ ultraviolet spectrometry of the ISUS nitrate sensor were calibrated against analysed nitrate concentrations [ $r^2 = 0.95$ ;  $n = 491$ ]. The isotopic composition of nitrate ( $\delta^{15}\text{N}$  and  $\delta^{18}\text{O}$ ) was measured by the bacterial denitrification method (Sigman et al., 2001) at the University of California Davis Stable Isotope Facility, according to standard methods (Casciotti et al., 2002; García and Gordon, 1992). We used  $\text{NO}$  as a conservative water mass tracer and calculated it using the formula  $9\text{NO}_3 + \text{O}_2$ , as each mole of consumed  $\text{O}_2$  will roughly release 1/9th of a mole bound N as a nitrate ion (Broecker, 1974; Whitney et al., 2007).

## 2.2 Other related data sets

ARGO float data along  $21^\circ\text{S}$ , including temperature, salinity, and oxygen data collected within 50 km of that latitude, were sourced from Integrated Marine Observing System (IMOS) via the ARGO website (<http://www.argo.ucsd.edu>, <http://argo.jcommops.org>).

An earlier transit through the region on the RV *Southern Surveyor* about one month prior to our major research voyage (April 2010) was used to visit the Sandy Bay transect ( $\sim 22^\circ\text{S}$ ). We sampled five CTD stations from the surface to 10 m above bottom, starting inshore at  $\sim 30$  m depth and continuing to the 1000 m isobaths. Nutrient and chlorophyll *a* samples (total) were taken at 10 depths at each of these five stations as described earlier.

## 3 Results

### 3.1 Early transit voyage

Early in the austral autumn (6–13 April 2010), during a transit voyage through the study region in May (Fig. 1a), surface waters were relatively fresh (35) compared to subtropical water, STW (35.8), and well mixed to  $\sim 150$  m based on CTD casts. Nitrate concentrations in the 35-salinity layer were  $0\text{--}10 \mu\text{mol L}^{-1}$ , with the highest values near shore. No clear LDOHN regions were visible, nor were there any subsurface salinity minima, as seen during the primary research voyage in May 2010. North of Northwest Cape, a regional

bloom of the nitrogen-fixing cyanophyte *Trichodesmium* was identified as distinctive pink-orange surface slicks reaching  $20^\circ\text{S}$ . This was a regional-scale feature during the April voyage (Fig. 1b)

### 3.2 Primary research voyage

During the primary cruise in May 2010, we identified several regional water masses and currents occurring in the study region (Domingues et al., 2007; Woo and Pattiaratchi, 2008) including subtropical water (STW; salinity  $\sim 35.2$ ) entering from the southwest, Eastern Gyral Current (EGC; salinity  $\sim 34.8$ ) waters entering from the west and northwest, and Leeuwin Current/Indonesian Throughflow (LC/ITF; salinity  $\sim 35.6$ ) from the north and northeast (Fig. 1a). Low dissolved oxygen high-nitrate (LDOHN) layers, whose overall importance had been established in our previous work (Thompson et al., 2011; Rossi et al., 2013), were visible between 100 and 250 m. These layers appeared as sharp gradients in both dissolved nitrate and oxygen with depth, associated specifically with low salinity waters (Fig. 2a–e). The profiles indicated local maxima in density gradients immediately above these layers (e.g.  $\Delta\rho = 0.025 \text{ kg m}^{-3}$ ; Fig. 2a–e) above which appeared a local minimum in transparency (Figs. 2b and 3a–b), correlated with increased particle concentration (Karageorgis et al., 2008). The LDOHN layers therefore occurred immediately below, sometimes partially overlapping, high particle loads as indicated by low transmission (Figs. 2a–e and 3b; red arrow). However, where low transmission occurred without low salinity (i.e. not adjacent to a density interface), it was not associated with a local nitrate peak (Fig. 3a; black arrow).

$TCO_2$  increases and  $\text{O}_2$  minima were associated with the lowest pH values observed in surface waters (Fig. 2e; Fig. 4a–b). Low  $\text{O}_2$  values were associated with peaks in nitrate concentration, but each nitrate peak showed a slightly different oxygen concentration (Fig. 5, note variations in blue/purple shading at nitrate peaks). These peaks co-occur with  $TCO_2$  maxima, such that

$$\text{Oxygen}(\mu\text{mol kg}^{-1}) = -0.52 \cdot TCO_2(\mu\text{mol kg}^{-1}) + 1237$$

$$(r = -0.80; n = 59; p < 0.0001).$$

However, the low-oxygen/high-nitrate anomalies did appear at many different densities between  $\rho = 24\text{--}26 \text{ kg m}^{-3}$ , along the mixing lines between STW and EGC, and even up into the LC waters (Fig. 3b), all associated with low transmission. These anomalies are regional in scale ( $\sim 1000$  km; Figs. 4b and 6). Oxygen data along  $21^\circ\text{S}$  from the ARGO floats showed that the low oxygen layers identified in the boundary region of the eastern Indian Ocean off Western Australia continued west as far as  $104^\circ\text{E}$  and even to  $102^\circ\text{E}$ , at a similar depth range as seen in the cruise data (Fig. 6).

When we combine the  $\text{O}_2$  and  $\text{NO}_3$  signatures as  $\text{NO}$  and compare with potential temperature, we correct for the

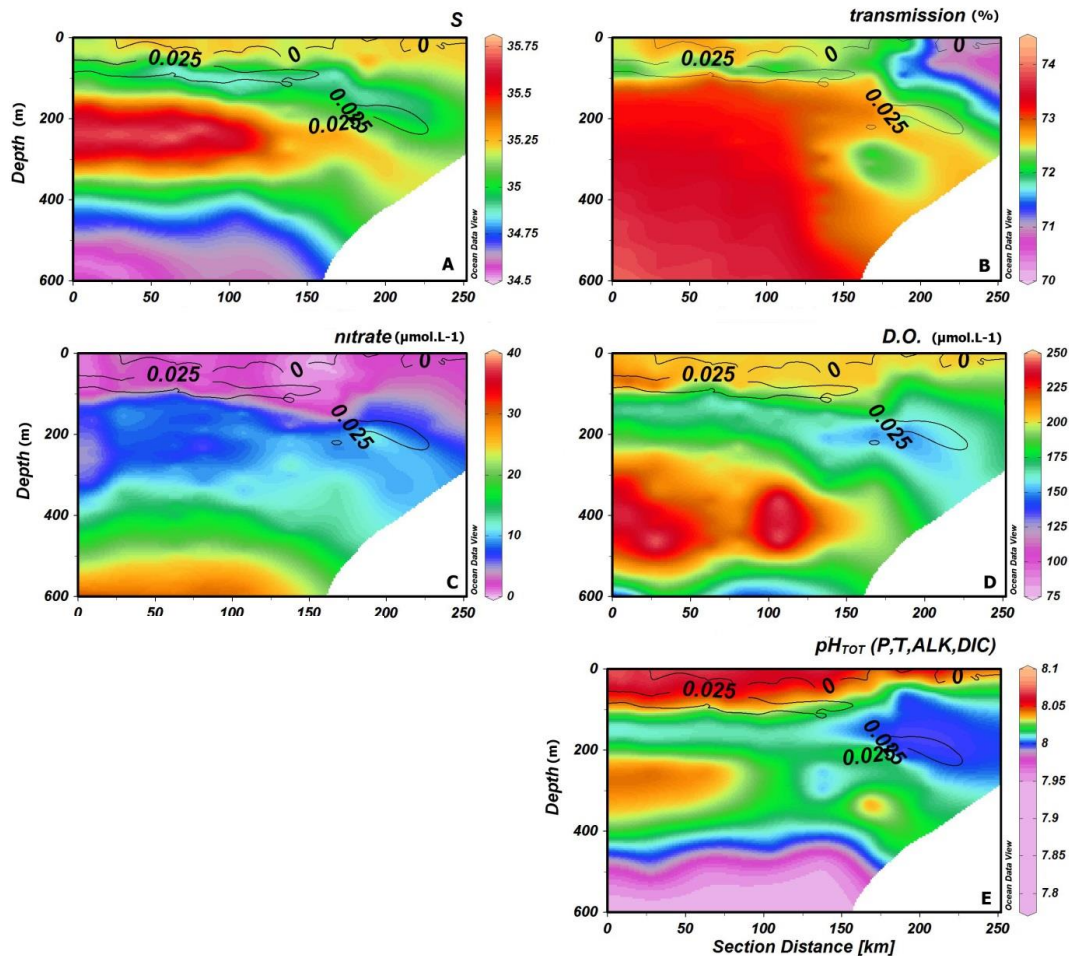


**Fig. 2.** (A–E) Longitudinal depth profiles along 21° S transect: (A) salinity with major water masses (LC, Leeuwin Current; EGC, Eastern Gyral Current; STW, subtropical water). Black contour lines in all panels represent the in situ density interface as the first derivative of density with depth ( $d/dz\rho$ ), whose maximum occurs at  $\Delta\rho = 0.025 \text{ kg m}^{-3}$ . (B) % transmission, with a path length of 25 cm at 660 nm (lower values indicate higher particle concentrations); (C) nitrate concentrations in  $\mu\text{mol L}^{-1}$ ; (D) dissolved Oxygen concentrations in  $\mu\text{mol L}^{-1}$ ; black arrow indicating low oxygen layer; and (E) pH, derived from total alkalinity and dissolved inorganic carbon.

change in gas solubility with depth (Broecker, 1974; Whitney et al., 2007), and the shallower nitrate peaks become more obvious as upward deflections of the black iso-nitrate contours (Fig. 7). The shallow high-nitrate anomalies occur at several distinct potential temperatures:  $\text{pot}T = 21, 23,$  and  $25^\circ\text{C}$ , which are all within the density range  $\rho = 24\text{--}26 \text{ kg m}^{-3}$ , and all at locally low salinities ( $\sim 35$ ). NO increases are driven locally by nitrate increases in each layer and are particularly marked at  $\text{pot}T = 25^\circ\text{C}$  and at 100–150 m depth. The multiple LDOHN layers we identified all occurred at lower than ambient salinities  $\sim 35$ , but at a wide range of temperatures and densities.

Critical to a deeper understanding of the processes controlling production in the region is an understanding of the origin of these subsurface nitrate maxima consistently observed within the study area in April–May (Thompson et al., 2011; Rossi et al., 2013). The isotopic signature of the dissolved

nitrate shows two clearly separated groups of  $\delta^{18}\text{O}$ .  $\delta^{18}\text{O}$  of surface nitrate is highly enriched ( $\delta^{18}\text{O} \sim 20\text{‰}$ ) while the  $\delta^{18}\text{O}$  of deep nitrate is significantly less ( $\delta^{18}\text{O} \sim 10\text{‰}$ ; 200–1000 m) (Fig. 8a). Consequently, the  $\delta^{18}\text{O}$  value of nitrate decreased significantly with depth ( $p < 0.001$ ;  $r^2 = 0.46$ ;  $n = 29$ ); this trend was significant across all Groups 1, 2, and 3 below.

The  $\delta^{15}\text{N}$  of deep nitrate was uniformly  $\sim 6\text{--}7\text{‰}$  at 200–1000 m (Fig. 8a). However, nitrate closer to surface contained two groupings according to  $\delta^{15}\text{N}$  – one with the deep nitrate signature of  $\sim 6\text{--}7\text{‰}$ , and another small cluster of points where  $\delta^{15}\text{N} = -1\text{--}2\text{‰}$  (Fig. 8a). Overall the DIN was grouped into three separate pools: Group 1, which has low  $\delta^{15}\text{N}$  ( $-1\text{--}4\text{‰}$ ) and high  $\delta^{18}\text{O}$  ( $\sim 22\text{‰}$ ); Group 2, which has the most enriched  $\delta^{15}\text{N}$  ( $7\text{--}11\text{‰}$ ) and high  $\delta^{18}\text{O}$  ( $\sim 22\text{‰}$ ); and Group 3, which has high  $\delta^{15}\text{N}$  ( $\sim 6.6\text{‰}$ ) and low  $\delta^{18}\text{O}$  ( $\sim 10\text{‰}$ ) (Fig. 8a). We then calculated two derived

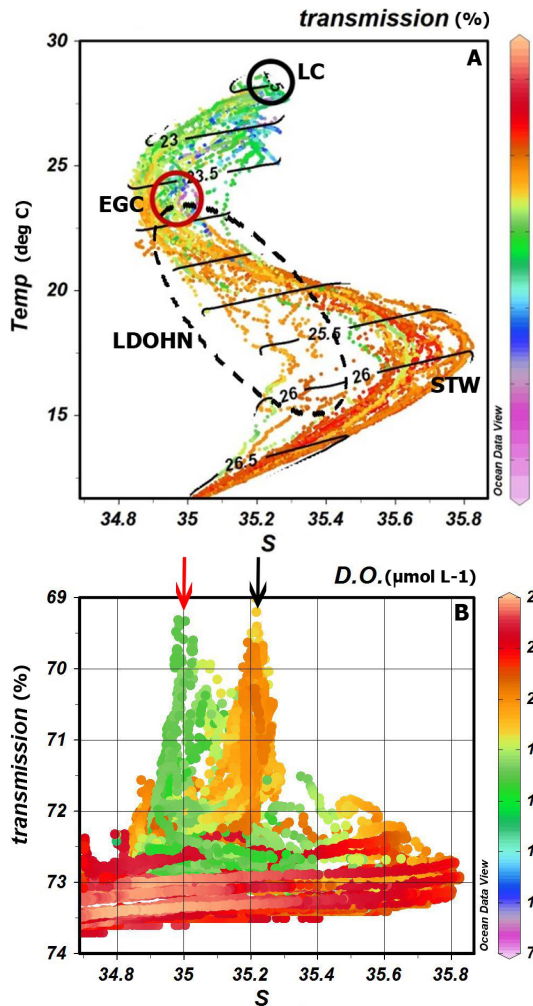


**Fig. 3.** Identifying particle-rich layers: **(A)** temperature (°C) vs. salinity plot with density contours, showing high salinity subtropical water (STW) beneath tropical waters of the fresher Eastern Gyral Current (EGC) overlain with warmer, more saline Leeuwin Current waters at the surface (LC), probably sourced from the Indonesian Throughflow (ITF). Transmission is indicated as dot colour. Transmission minima (maxima of particle concentrations) are seen within the forming Leeuwin Current (LC) waters ( $T = 28^{\circ}\text{C}$ ,  $\text{Sal} = 35.3$ ) and the Eastern Gyral Current (EGC), which is cooler and fresher ( $T \sim 24^{\circ}\text{C}$ ,  $\text{Sal} \sim 34.9$ ). LDOHN layers are visible between  $\rho = 24$  and  $26 \text{ kg m}^{-3}$ , showing salinity profiles scattered between  $\rho = 24$  and  $26.5 \text{ kg m}^{-3}$  (dashed oval). **(B)** Relationship between transmission and salinity with dissolved oxygen ( $\mu\text{mol L}^{-1}$ ) as dot colour. Note that the two transmission minima, at salinity  $\sim 35$  and  $\sim 35.2$ , just offset from the LC and EGC water properties. The maximum at  $\text{Sal} = 35$  is a major LDOHN layer whose intrusion creates the  $\Delta\rho = 0.025 \text{ kg m}^{-3}$  anomaly (Fig. 1) (indicated with red arrow; see also red circle in Fig. 4), with nitrate concentrations  $\sim 2\text{--}10 \mu\text{mol L}^{-1}$ . Black arrow indicates more saline, warmer waters of the Leeuwin Current, in which nitrate has not been generated despite high transmission; oxygen remains high (see black circle, Fig. 4). Both peaks have relatively low NO properties, but in the fresher peak has a much higher nitrate : oxygen ratio (see also Fig. 6).

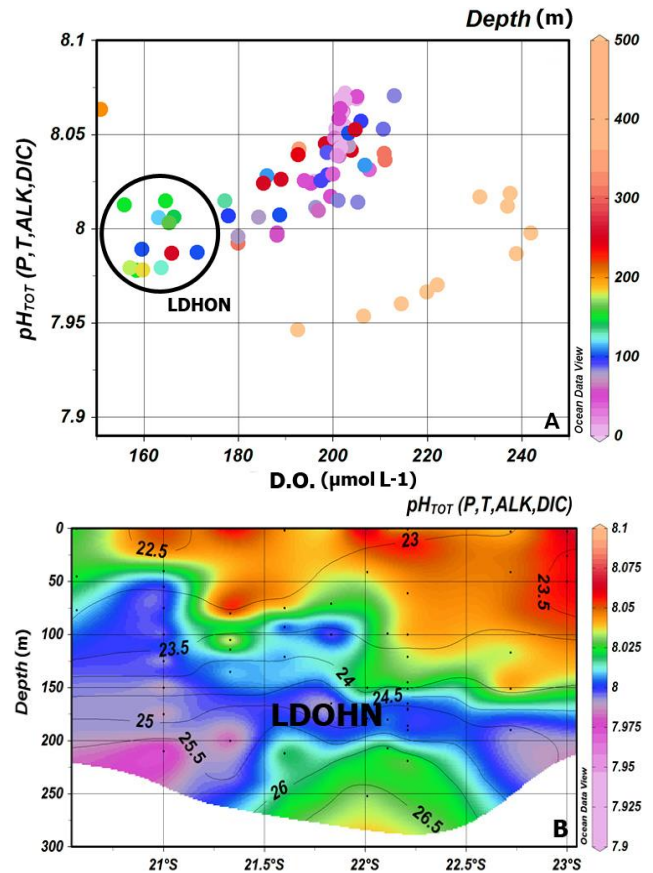


**Fig. 4.** **(A)** pH declines with lower oxygen concentrations in waters shallower than 200 m, such that pH minima occur where oxygen concentrations are  $< 160 \mu\text{mol L}^{-1}$ . Note that there are two separate relationships between oxygen and pH: one shallower than 200 m and one below 400 m depth. **(B)** Meridional pH anomaly along the  $\sim 200 \text{ m}$  contour (roughly  $114\text{--}113.5^{\circ}\text{E}$ ) across the study region.

terms from the  $\delta^{15}\text{N}$  values: (i) for Group 1, where  $\delta^{15}\text{N}$  nitrate values were between  $-1$  and  $4\text{‰}$ , we estimated the percent of the nitrate signal attributable to nitrogen fixation, using a simple linear mixing model with two end points, assuming a  $\delta^{15}\text{N} = -1\text{‰}$  for N-fixation (Montoya et al., 2002) and  $\delta^{15}\text{N} = 6.6\text{‰}$  for deep nitrification (Waite et al., 2007a) (Fig. 8b). These values decreased from 97 % at the surface to 0 % at  $\sim 200 \text{ m}$  and were strongly correlated with depth ( $r^2 = 0.52$ ;  $n = 12$ ).

(ii) For Group 2, the observed  $\delta^{15}\text{N}$  values of nitrate were consistent with zooplankton-grazing signatures documented elsewhere (Montoya et al., 2002). We therefore investigated the implication of our measured values by calculating an estimated “trophic enrichment factor” (TEF) measuring the shift towards higher  $\delta^{15}\text{N}$  values from an assumed deep nitrate baseline ( $\text{TEF} = X - 6.7\text{‰}$ ) for each value. We then calculated a nominal trophic level (TL) for the produced nitrate, based on trophic relationships established by Waite et al. (2007a) for extremely low nitrogen environments in

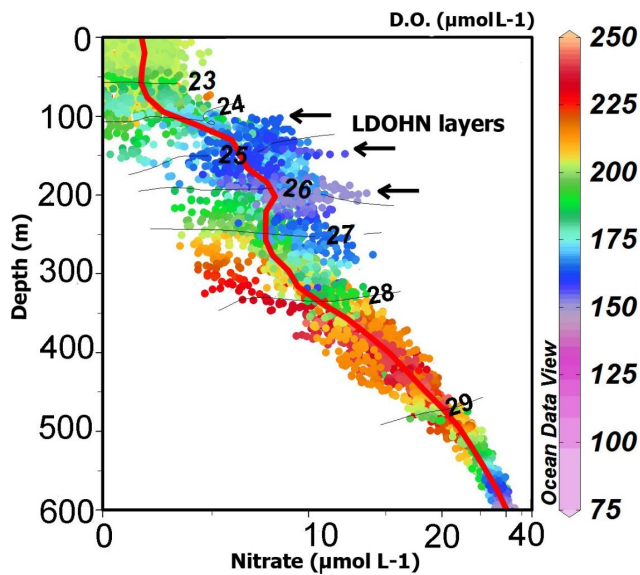


**Fig. 5.** Depth profile plot of nitrate concentrations with dissolved oxygen concentrations overlay and in situ density contour lines in black, from 21° S transect. Several LDOHN layers are visible just below the  $\rho = 24 \text{ kg m}^{-3}$  density isoline, and between  $\rho = 25\text{--}26 \text{ kg m}^{-3}$  isolines (black arrows) and below  $\rho = 27 \text{ kg m}^{-3}$ . Note that oxygen is locally lowered below saturation in each LDOHN layer, but each layer has a different characteristic oxygen signal (seen as varying pale blue, dark blue and purple shading of dots). Data from transect 1 (Fig. 1f) were fitted through piece-wise linear least squares function.

the eastern Indian Ocean. This study showed a  $\delta^{15}\text{N}$  enrichment of  $\sim 2.2\%$  per trophic level across several ecosystems and nitrogen sources. Local reef fish had also shown a  $\delta^{15}\text{N}$  enrichment of  $\sim 2.4\%$  (Wyatt et al., 2010). Note that the TEF  $\rightarrow$  TL calculation contains the embedded assumption that initial uptake values start with deep nitrate  $\delta^{15}\text{N} = 6.6\%$ , not fixed nitrogen, making this trophic enrichment estimate very much a minimum value (Fig. 8c). The calculated nominal TL values of  $\delta^{15}\text{N}$  nitrate ranged from a TL  $\sim 2.5\%$  in surface waters to TL  $\sim 0$  (i.e. unassimilated deep nitrate) at 250 m. TL decreased exponentially with depth ( $p < 0.01$ ;  $r^2 = 0.50$ ;  $n = 17$ ).

#### 4 Discussion

We suggest that spatial coupling between nitrate, transmission and oxygen across the study region indicates the presence of in situ respiration processes, which consume oxygen and re-mineralize particulate organic matter locally. These processes contribute to the development of low pH layers at interfaces (high vertical  $\Delta\rho$ ) created by the subduction of low salinity waters from the Eastern Gyral Current (EGC) into the water masses of the continental shelf region. Our evidence suggests that the production of these layers oc-

curs at small scales (100 m in the vertical) and on the short term (weeks). While the original source of organic matter could be oceanographically well upstream of the study region, especially given the large scale ( $10\,000 \text{ km}^2$ ) of the *Trichodesmium* bloom observed a month previously, organic matter sources could also be more local. In the present study, we show the accumulation of organic matter at the interface of LDOHN layers, as we had previously speculated might occur (Rossi et al., 2013). In situ local biogeochemical processes (surface nitrogen fixation followed by sinking/subduction, decomposition and nitrification of the biomass) are major contributors to the formation, and maintenance of the subsurface nitrate maxima, although the advection by oceanic currents of peculiar biogeochemical characteristics also plays a role.

#### 4.1 Oceanographic history and formation of LDOHN layers

A transit voyage in April 2010 anecdotally observed salinities at the surface that were consistent with EGC waters. These waters had low but detectable dissolved nitrate concentrations (generally  $\sim$  detection limit  $= 0.05 \mu\text{mol L}^{-1}$ ), as well as a visible bloom of the N-fixing Cyanobacterium *Trichodesmium* to the north, covering  $100 \times 100$  square kilometres (Fig. 1b–c; A. Waite, unpublished data). The seasonal acceleration of warm, more saline Leeuwin Current surface water (though still less saline than the STW) in the austral autumn (Domingues et al., 2007) observed in this study is therefore likely to have occurred regionally in the intervening month, subducting the lower salinity EGC layer beneath it (see schematic in Fig. 9). The deeper boundary of the low salinity layer(s) seems to then have become a “hotspot” (sensu Doostmohammadi et al., 2012) for remineralization of particulate organic matter, originating to a large part from  $\text{N}_2$  fixation. Our analysis, including the observation of multiple LDOHN layers with distinctive oxygen signatures, suggests further complex interleaving of water masses of different temporal origins, possibly with different oxygen histories.

North of this region, The WOCE data set (e.g. IR10 [http://www-pord.ucsd.edu/whp\\_atlas/indian/i10/prop\\_plots](http://www-pord.ucsd.edu/whp_atlas/indian/i10/prop_plots)) suggests that surface waters with salinity of  $\sim 35$  occur in general north of  $15^\circ \text{ S}$  for most of the year, and are a likely source for the low salinity layer we observed, including cool and variable temperatures, low dissolved oxygen and total alkalinity ( $2280\text{--}2300 \mu\text{mol kg}^{-1}$  at  $20\text{--}25^\circ \text{ C}$ ). Property plots also show low dissolved oxygen associated with high nitrate values, originating from the north as far as  $10^\circ \text{ S}$  on the WOCE IR10 line and east into the Indonesian Through-flow (ITF) region (WOCE line IR6C). Wijffels et al. (2002) suggest that the ITF carries the high-nutrient low-oxygen signal from the shallow waters off Indonesia, and that this water mass becomes more saline as it recirculates westward, before flowing eastward to form the Leeuwin Current (LC).

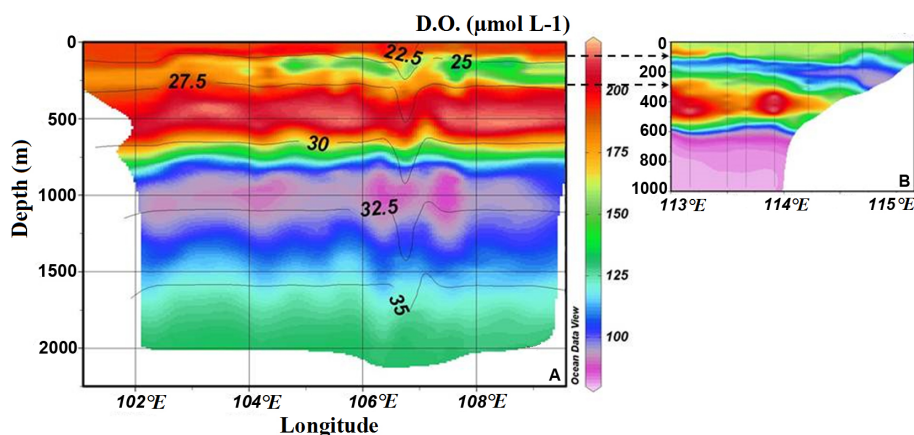


**Fig. 6.** Dissolved oxygen concentrations in  $\mu\text{mol L}^{-1}$  along  $21^\circ\text{S}$ . **(A)** Compilation of all available regional oxygen data from profiling Argo floats, showing that the oxygen minimum is regional in scale, centred just above 200 m. **(B)** Primary research cruise data from  $21^\circ\text{S}$  (adapted from Fig. 1d) match, spatially, reasonably well with the Argo data despite very different spatial and temporal scales.

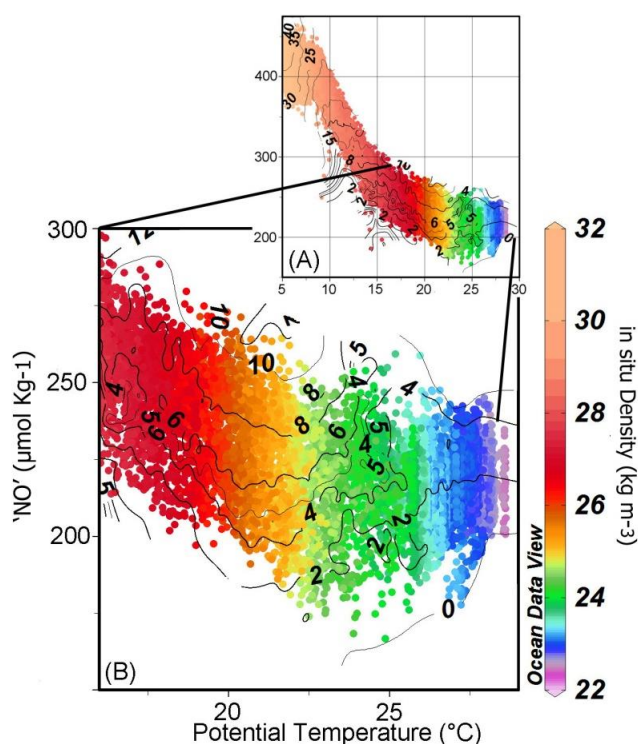


**Fig. 7.** Plot of “NO” ( $\mu\text{mol kg}^{-1}$ ) versus potential temperature with in situ density overlay and nitrate concentration contour lines in black from all the data collected in the study area. LDOHN layer at  $\rho = 24\text{ kg m}^{-3}$  density isoline, with peaks at  $\rho = 25\text{--}26\text{ kg m}^{-3}$  isoline. Sharp increase in nitrate concentrations from  $\sim 2$  to  $5\text{--}10\text{ }\mu\text{mol L}^{-1}$  within 10–20 m.

Later work has shown that both Indian and Indonesian tropical sources are important in forming the LC, but that different recirculation times of ITF waters between Australia and Indonesia (the so-called “S” and “C” trajectories) result

in markedly different  $T/S$  properties further south in the forming LC (Domingues et al., 2007). The  $S$  trajectories provide the freshest and warmest water source to  $22^\circ\text{S}$ , entering the LC system at the surface and in the eastern sector of the LC formation region, while the  $C$  trajectories enter the LC formation region slightly further west (offshore) and slightly deeper (Domingues et al., 2007). The May–June austral autumn acceleration of the Leeuwin Current (LC) seems to favour sources from the longer  $S$  route (Domingues et al., 2007). The LC waters in our study appear similarly close to the Western Australian coast, and at the surface, suggesting that the surface waters we observed are also likely to have originated from the  $S$  route.

The Eastern Gyral Current (EGC) emerges as a key player in the formation of LDOHN layers. The EGC forms from a retroflection of the South Equatorial Current, but loses heat in the tropical–subtropical transition area before a significantly cooled and slightly more saline branch moves south towards Northwest Cape at about  $22^\circ\text{S}$  (Domingues et al., 2007). It is these waters that are subducted by the LC waters of varying salinities that accelerate SW along the Australian northwest shelf during the austral autumn (May–June). Our observations near Sandy Bay, Northwest Cape ( $\sim 22^\circ\text{S}$ ), about 1 month earlier in April show EGC waters from the surface to about 100 m. By May, the EGC waters were subducted in a complex series of layers beneath the LC waters. We suggest that this puts a 3–4 week timeline on the formation of LDOHN layers, consistent with the  $\sim 1$  month timeline estimated to advect the interleaving water masses southward by  $2\text{--}4^\circ$  of latitude (Domingues et al., 2007).

#### 4.2 Sources of particles

Remineralization will be optimized if sources of organic matter from the surface are available for export, accumulating at strong interfaces (Macintyre et al., 1995). The low

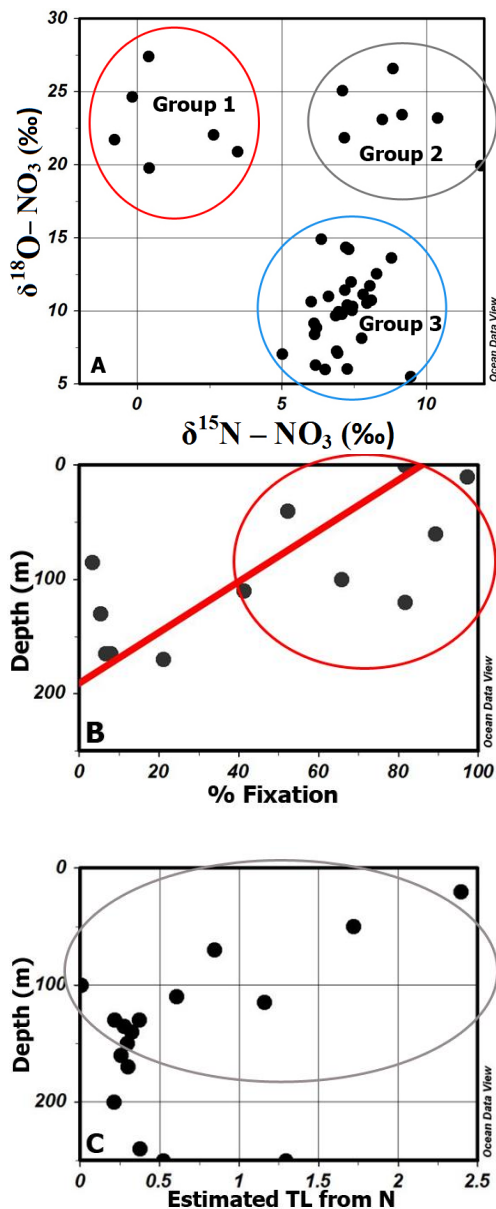


**Fig. 8.** Isotopic composition of dissolved nitrate across the study region. (A)  $\delta^{15}\text{N}$  near or below zero is classic evidence of nitrogen fixation as an N source, while deep nitrate classically has a regional signature of  $\sim 6.60$  ‰. Near-surface  $\delta^{18}\text{O}$  sources are known to be enriched in  $\delta^{18}\text{O}$  due to preferential evaporation of  $^{16}\text{O}$  over  $^{18}\text{O}$ . Group 1: nitrate produced using fixed nitrogen and surface oxygen (red circle) Group 2: nitrate produced using surface oxygen and nitrogen from non-fixation sources, likely to be grazing (Montoya et al., 2002) (black circle) Nitrate produced at depth conforming to the regional mean of  $\delta^{15}\text{N} = 6.60$  ‰ (Waite et al., 2007a) (blue circle). (B) Derived value for % of nitrate originating from nitrogen fixation calculated with a simple linear isotope mixing model, with a fixation end point  $\delta^{15}\text{N} = -10$  ‰, and deep regenerated nitrate  $\delta^{15}\text{N} = 6.60$  ‰. (C) Speculative estimation of the source trophic level (TL) of regeneration for the measured nitrate – based on the  $\Delta\delta^{15}\text{N}$  of 2.2 ‰ per trophic level we estimated for the oligotrophic Indian Ocean by Waite et al. (2007a); see text for details.

transmission properties of waters within and immediately above the LDOHN layers suggest the existence of a significant supply of organic matter. We initially speculated that dense-water formation originating from the shelf during the autumn/winter period, as documented further south (Pattiaratchi et al., 2011), could play a role in contributing to particle movement offshore (Rossi et al., 2013). Our data feature significant near-shore sources of particles which could theoretically drive significant oxygen depletion ( $70 \mu\text{mol kg}^{-1}$ ; Fig. 4a) in LDOHN layers. However, we also observed low-transparency, particle-rich layers (Karageorgis et al., 2008) at multiple locations within the mixing line between the Eastern Gyral Current waters and the more saline STW, which moves shorewards from the southwest, penetrating deeper and more regionally beneath the EGC and the forming Leeuwin Current (Waite et al., 2007b). This implies that offshore sources of particles are also likely to be important in the formation of LDOHN layers. This might help explain the apparent continuity of LDOHN layers as far west as  $102\text{--}104^\circ \text{E}$ . Once organic-rich waters are subducted under the Leeuwin Current, particles could continue to accumulate on the resulting density interface(s), favouring continued and/or increasing microbial regeneration there. Okubo's analysis of  $^{234}\text{Th}$ -based particle fluxes with depth at two stations along  $110^\circ \text{E}$  in the eastern Indian Ocean also suggested rapid remineralization of organic matter was occurring in the top 250 m (Okubo et al., 2007).

Remineralization rates are often controlled by fluctuations in the availability of oxidizable organic matter (Farias et al., 2007). Phytoplankton in coastal regions are known to accumulate as sinking aggregates at density interfaces (Allredge et al., 2002), but less is known about the prevalence of such processes in the open ocean. Most mechanistic analyses of low-oxygen layers necessarily assume a close coupling of particle hydrolysis and uptake of hydrolysates by bacteria, followed by remineralization (Pantoja et al., 2004). Microbial populations accumulate at pycnoclines, experiencing what Stocker (2012) refers to as the ocean's "microarchitecture" and responding physiologically to its associated strong chemical gradients. Microbes can both respond to these gradients (Taylor and Stocker, 2012) and become physically trapped by them (Doostmohammadi et al., 2012). Strong pycnoclines are therefore likely to become biogeochemical "hotspots" (Doostmohammadi et al., 2012) where particle accumulation, remineralization and microbial activity are all likely to be elevated. In our study, we found that low-transmission particle-rich layers were closely associated with lower oxygen concentrations (e.g. Fig. 3) and high nitrate concentrations (e.g. Fig. 5). In fact our LDOHN layers seem overall to be analogous to the "upper oxycline" found in the shallow part of the oxygen minimum zones off Chile, where nitrification drives a peak of nitrate production well above the oxygen minimum.

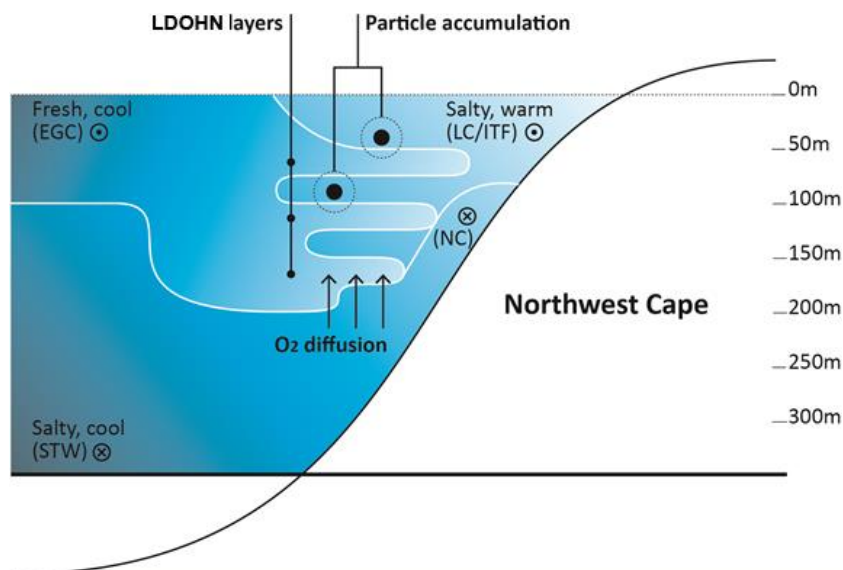


**Fig. 9.** Schematic of formation of LDOHN layers in the autumn off Northwest Cape, Western Australia. The fresh, cool water from the northwest (e.g. the Eastern Gyral Current, EGC) interweaves with arrival events of the more salty, warmer Leeuwin Current (LC) source waters from the Indonesian Throughflow (ITF) in the late summer and autumn. Periodically, the Ningaloo Current (NC) is formed near the coast due to strong southwesterly winds. The LDOHN layers, containing locally high nitrate and high dissolved organic carbon, as well as low oxygen and low pH, form beneath particle-rich layers sourced variously from surface waters and dependent on local surface production for supply of particles. Nitrogen fixation accounts for a measurable fraction of the nitrate generated in LDOHN waters, but seems to be rapidly transformed, taken up and remineralized, likely by microheterotrophs.

If we assume that a  $70 \mu\text{mol kg}^{-1}$   $\text{O}_2$  deficit requires an injection of at least  $70 \mu\text{mol particulate C L}^{-1}$  (or  $70 \text{mmol m}^{-3}$ ) to be generated, a conservative LDOHN layer depth of 25 m would require a vertical flux of  $1750 \text{mmol m}^{-2}$  or  $146 \text{mg m}^{-2}$ . Recent offshore production estimates are on the order of  $\sim 200 \text{mg C m}^{-2} \text{d}^{-1}$  (Hanson et al., 2005), suggesting that local production rates could sustain a carbon flux of  $35 \text{mg C m}^{-2} \text{d}^{-1}$  ( $F$  ratio = 0.1–0.2) on a daily basis if remineralization percentages over the top 200 m of ocean are similar to those found in regions supporting oxygen anomalies elsewhere ( $\sim 80\%$ ; Farias et al., 2007), especially if particles are concentrated on a density interface. This would put the timescale for generation of the LDOHN layer on the order of 4–5 days. Respiration values of  $0.4$  to  $3.6 \mu\text{mol L}^{-1} \text{d}^{-1}$  (Odate et al., 2002) would generate a  $70 \mu\text{mol kg}^{-1}$   $\text{O}_2$  deficit in  $\sim 20$ – $175$  days, depending on assumptions. These timescales would imply inputs from a spatial scale of  $\sim 100$  km as the catchment for organic carbon supporting the oxygen depletion. Our observation of the nitrogen-fixing bloom  $\sim 1$  month before we measured a low  $\delta^{15}\text{N}$  in the observed LDOHN (see below) would put the timescale at a maximum of about 30 days.

### 4.3 Isotopic sources of oxygen and nitrogen

Oxygen and nitrogen isotope signals are coupled through nitrification, and de-coupled in the euphotic zone through nitrate assimilation by algae, with the release of oxygen into

surface waters and formation of organic nitrogen (Sigman et al., 2009). Dissolved oxygen contributes  $\text{O}_2$  at  $\sim 24\%$ , while water has an oxygen signature closer to 0. The deeper values of  $\text{NO}_3 \delta^{18}\text{O}$  we measured,  $\sim 10\%$ , suggest that at least one of 6 O's in nitrate originate from locally dissolved oxygen, not water (Sigman et al., 2009). Our surface  $\delta^{18}\text{O}$  values in surface nitrate are high compared to literature values (Sigman et al., 2005), but consistent with modelling outputs for the surface ocean (Sigman et al., 2009); it is possible that  $\text{O}_2$  fractionation during consumption associated with high community respiration rates has increased the baseline  $\delta^{18}\text{O}$  of  $\text{O}_2$  available for nitrification. This would be consistent with our observation that oxygen levels in this region are lower than many other areas of the world ocean. Our groups of high and low  $\delta^{18}\text{O}$  values thus suggest surface and deep sources of nitrate respectively.

The deep  $\delta^{15}\text{N}$  values of  $\text{NO}_3$  cluster around the mean deep values of  $\sim 6.7\%$  measured in the eastern Indian Ocean (Waite et al., 2007a), about  $2\%$  higher than the mean value of  $5\%$  commonly used for the world ocean. Near the surface we find two distinct pools of nitrate that are spatially scattered throughout the study region. One set of values shows nitrate increasing in  $\delta^{15}\text{N}$  towards the surface, consistent with a grazing signal, and another shows values of  $\delta^{15}\text{N}$  decreasing towards the surface, reaching a minimum value of  $-2\%$ , which is consistent with nitrogen fixation. Though alternative interpretations have been suggested (Knapp et al.,

2011), fixation remains the most plausible source of this signal.

Our separation of nitrogen sources into three isotopic groups based on  $\delta^{15}\text{N}$  and  $\delta^{18}\text{O}$  then allows us to distinguish dissolved nitrate originating from nitrogen fixation and formed at the surface (Group 1), and nitrate likely to have been assimilated, and then released as DON by grazers at the surface and nitrified (Group 2). We estimate that 97% of unassimilated nitrate (Group 1) found in surface waters of the region is likely to have originated from nitrogen fixation. This suggests that N-fixation had recently been a major contributor to local production (Sigman et al., 2009). The observation of a massive bloom of *Trichodesmium* in the same area 30 days previously confirms that such sources did exist locally. At that time, the LDOHN layer was not clearly observable in this area. This again seems to set a timeline of days to weeks for the formation and maintenance of the LDOHN layer. In addition, it suggests offshore, surface-ocean particle sources are also likely to be strong contributors to remineralization sources for the LDOHN layers.

Our observations indicating N-fixation as an important nitrate source is coupled with some highly enriched isotopic values of nitrate-N (Group 2) in the immediate sub-surface (20 m) suggest simultaneous rapid assimilation via grazing, generating nitrate with a nominal trophic level of 2.4. This is remarkably similar to the effective trophic level of  $\sim 3$  calculated for surface microheterotrophs by Waite et al. (2007a), and suggests rapid recycling and remineralization occurs in this system, consistent with the high respiration rates suggested by the surface  $\delta^{18}\text{O}$ .

#### 4.4 The carbonate system

The pH minimum in the LDOHN layer, characterized by a peak in total DIC up to  $35\ \mu\text{mol kg}^{-1}$ , indicates that remineralization has occurred for long enough to decrease pH at the density interface. How low could this pH go? Theoretically, based on the observed relationships between oxygen, carbon, and pH in this system, we might expect oxygen to become fully depleted at a  $T\text{CO}_2$  value of  $2378\ \mu\text{mol kg}^{-1}$ , setting a limit of  $\text{pH} = 7.79 (\pm 0.04)$  in surface waters  $< 200$  m, and  $\text{pH} = 7.74 (\pm 0.02)$  in waters deeper than 300 m (see two separate relationships, Fig. 4a). However, we note that remineralization of organic matter from N-fixation could produce even greater pH decreases associated with the generation of excess protons during nitrification (Wolf-Gladrow et al., 2007). This would suggest that regions such as this one, where nitrate may be sourced significantly from N-fixation, may be more than usually exposed to changes in ocean pH.

#### 4.5 Regional implications

We note that in comparison to other ocean basins (Broecker, 1974), the region seems depleted in oxygen, with surface NO values as low as 175, well below those documented for the

open Atlantic and Pacific (Broecker, 1974). The deeper STW contains higher NO values than the LC, EGC, and associated LDOHN layers, and may contribute importantly to their oxygen budget. This, and the association of low oxygen and N-fixation-derived nitrification with low pH (above), heightens the importance of understanding regional controls of the oxygen budget and their impact on ecosystem dynamics in this poorly studied region of the Indian Ocean.

The stable layering of warm, salty water over cooler, fresher water in this region forms a system in which double diffusion might be expected to occur (Turner, 1973). There is tentative evidence of double diffusion of the diffusive-layering variety, but the implications of this on the biology and hydrography remain unclear (Kelley et al., 2003), and will need further exploration for this system.

*Acknowledgements.* We thank P. Grierson for helpful discussions regarding isotopic fractionation of oxygen, C. Domingues for helpful discussions on the interleaving water masses and D. Kelly for valuable insights into double diffusion. This study was supported by an Australian Research Council Discovery Project Grant #DP0663670 to A. M. Waite, M. Roughan, J. Kotta, H. Orav-Kotta, and C. Pattiaratchi. Ship time for both the primary voyage (V04-2010) and the earlier Transit Voyage (T01-2010) was supported by the Australian Marine National Facility. ARGO data were collected and made freely available by the International Argo Project and the national programmes that contribute to it (<http://www.argo.ucsd.edu>, <http://argo.jcommops.org>). The Argo Project is part of the Global Ocean Observing System. Australian Argo data were sourced from the Integrated Marine Observing System (IMOS). The ocean colour image of the *Trichodesmium* sp. bloom was also provided by IMOS. IMOS is supported by the Australian Government through the National Collaborative Research Infrastructure Strategy and the Super Science Initiative.

Edited by: U. Riebesell

#### References

- Allredge, A. L., Cowles, T. J., MacIntyre, S., Rines, J. E. B., Donaghay, P. L., Greenlaw, C. F., Holliday, D. V., Deksheniaks, M. M., Sullivan, J. M., and Zaneveld, J. R. V.: Occurrence and mechanisms of formation of a dramatic thin layer of marine snow in a shallow Pacific fjord, *Mar. Ecol.-Prog. Ser.*, 233, 1–12, doi:10.3354/meps233001, 2002.
- Broecker, W. S.: “NO”, a conservative water-mass tracer, *Earth Planet. Sc. Lett.*, 23, 100–107, doi:10.1016/0012-821x(74)90036-3, 1974.
- Casciotti, K., Sigman, D., Hastings, M. G., Böhlke, J., and Hilkert, A.: Measurement of the oxygen isotopic composition of nitrate in seawater and freshwater using the denitrifier method, *Anal. Chem.*, 74, 4905–4912, 2002.
- Codispoti, L. A.: An oceanic fixed nitrogen sink exceeding  $400\ \text{Tg N a}^{-1}$  vs the concept of homeostasis in the fixed-nitrogen inventory, *Biogeosciences*, 4, 233–253, doi:10.5194/bg-4-233-2007, 2007.

- Dickson, A. G.: Guide to Best Practices for Ocean CO<sub>2</sub> Measurements, PICES Special Publication 3, 191 pp., 2007.
- Domingues, C. M., Maltrud, M. E., Wijffels, S. E., Church, J. A., and Tomczak, M.: Simulated Lagrangian pathways between the Leeuwin Current System and the upper-ocean circulation of the southeast Indian Ocean, *Deep-Sea Res. Pt. II*, 54, 797–817, doi:10.1016/j.dsr.2006.10.003, 2007.
- Doostmohammadi, A., Stocker, R., and Ardekani, A. M.: Low-Reynolds-number swimming at pycnoclines, *P. Natl. Acad. Sci. USA*, 109, 3856–3861, doi:10.1073/pnas.1116210109, 2012.
- Farias, L., Paulmier, A., and Gallegos, M.: Nitrous oxide and N-nutrient cycling in the oxygen minimum zone off northern Chile, *Deep-Sea Res. Pt. I*, 54, 164–180, doi:10.1016/j.dsr.2006.11.003, 2007.
- García, H. E. and Gordon, L. I.: Oxygen solubility in seawater: Better fitting equations, *Limnol. Oceanogr.*, 37, 1307–1312, 1992.
- Gruber, N.: Warming up, turning sour, losing breath: ocean biogeochemistry under global change, *Philos. T. R. Soc. A*, 369, 1980–1996, doi:10.1098/rsta.2011.0003, 2011.
- Hanson, C. E., Pattiaratchi, C. B., and Waite, A. M.: Sporadic upwelling on a downwelling coast: Phytoplankton responses to spatially variable nutrient dynamics off the Gascoyne region of Western Australia, *Cont. Shelf Res.*, 25, 1561–1582, doi:10.1016/j.csr.2005.04.003, 2005.
- Johnson, K. M., Wills, K. D., Butler, D. B., Johnson, W. K., and Wong, C. S.: Coulometric total carbon dioxide analysis for marine studies: maximizing the performance of an automated continuous gas extraction system and coulometric detector, *Mar. Chem.*, 44, 167–187, 1993.
- Karageorgis, A. P., Gardner, W. D., Georgopoulos, D., Mishonov, A. V., Krasakopoulou, E., and Anagnostou, C.: Particle dynamics in the Eastern Mediterranean Sea: A synthesis based on light transmission, PMC, and POC archives (1991–2001), *Deep-Sea Res. Pt. I*, 55, 177–202, doi:10.1016/j.dsr.2007.11.002, 2008.
- Kelley, D. E., Fernando, H. J. S., Gargett, A. E., Tanny, J., and Ozsoy, E.: The diffusive regime of double-diffusive convection, *Prog. Oceanogr.*, 56, 461–481, doi:10.1016/s0079-6611(03)00026-0, 2003.
- Knapp, A. N., Sigman, D. M., Lipschultz, F., Kustka, A. B., and Capone, D. G.: Interbasin isotopic correspondence between upper-ocean bulk DON and subsurface nitrate and its implications for marine nitrogen cycling, *Global Biogeochem. Cy.*, 25, GB4004, doi:10.1029/2010gb003878, 2011.
- Macintyre, S., Alldredge, A. L., and Gotschalk, C. C.: Accumulation of marine snow at density discontinuities in the water column, *Limnol. Oceanogr.*, 40, 449–468, 1995.
- Montoya, J. P., Carpenter, E. J., and Capone, D. G.: Nitrogen fixation and nitrogen isotope abundances in zooplankton of the oligotrophic North Atlantic, *Limnol. Oceanogr.*, 47, 1617–1628, 2002.
- Odate, T., Furuya, K., and Fukuchi, M.: Photosynthetic oxygen production and community respiration in the Indian sector of the Antarctic Ocean during austral summer, *Polar Biol.*, 25, 859–864, 2002.
- Okubo, A., Obata, H., Luo, S., Gamo, T., Yamamoto, Y., Minami, H., and Yamada, M.: Particle flux in the twilight zone of the eastern Indian Ocean: A constraint from U-234-Th-230 and Ra-228-Th-228 disequilibria, *Deep-Sea Res. Pt. I*, 54, 1758–1772, doi:10.1016/j.dsr.2007.06.009, 2007.
- Pantoja, S., Sepulveda, J. S., and Gonzalez, H. E.: Decomposition of sinking proteinaceous material during fall in the oxygen minimum zone off northern Chile, *Deep-Sea Res. Pt. I*, 51, 55–70, doi:10.1016/j.dsr.2003.09.005, 2004.
- Parsons, T. R., Maita, Y., and Lalli, C. M.: Manual of chemical and biological methods for seawater analysis, Pergamon, 1984.
- Pattiaratchi, C., Hollings, B., Woo, M., and Welhena, T.: Dense shelf water formation along the south-west Australian inner shelf, *Geophys. Res. Lett.*, 38, L10609, doi:10.1029/2011gl046816, 2011.
- Rossi, V., Feng, M., Pattiaratchi, C. B., Roughan, M., and Waite, A. M.: Linking synoptic forcing and local mesoscale processes with biological dynamics off Ningaloo Reef, *J. Geophys. Res.*, 118, 1211–1225, 2013.
- Siegenthaler, U. and Sarmiento, J. L.: Atmospheric Carbon-Dioxide and the Ocean, *Nature*, 365, 119–125, 1993.
- Sigman, D. M., Casciotti, K. L., Andreani, M., Barford, C., Galanter, M., and Bohlke, J. K.: A bacterial method for the nitrogen isotopic analysis of nitrate in seawater and freshwater, *Anal. Chem.*, 73, 4145–4153, 2001.
- Sigman, D. M., Granger, J., DiFiore, P. J., Lehmann, M. M., Ho, R., Cane, G., and van Geen, A.: Coupled nitrogen and oxygen isotope measurements of nitrate along the eastern North Pacific margin, *Global Biogeochem. Cy.*, 19, GB4022, doi:10.1029/2005gb002458, 2005.
- Sigman, D. M., DiFiore, P. J., Hain, M. P., Deutsch, C., Wang, Y., Karl, D. M., Knapp, A. N., Lehmann, M. F., and Pantoja, S.: The dual isotopes of deep nitrate as a constraint on the cycle and budget of oceanic fixed nitrogen, *Deep-Sea Res. Pt. I*, 56, 1419–1439, doi:10.1016/j.dsr.2009.04.007, 2009.
- Stocker, R.: Marine Microbes See a Sea of Gradients, *Science*, 338, 628–633, 10.1126/science.1208929, 2012.
- Takahashi, T., Sutherland, S. C., Wanninkhof, R., Sweeney, C., Feely, R. A., Chipman, D. W., Hales, B., Friederich, G., Chavez, F., Watson, A., Bakker, D. C. E., Schuster, U., Metzl, N., Yoshikawa-Inoue, H., Ishii, M., Midorikawa, H., Sabine, C., Hoppema, M., Olafsson, J., Arnarson, T. S., Tilbrook, B., Johannessen, T., Olsen, A., Bellerby, R., de Baar, H. J. W., Nojiri, Y., Wong, C. S., Delille, B., and Bates, N. R.: Climatological Mean and Decadal Change in Surface Ocean *p*CO<sub>2</sub>, and Net Sea-air CO<sub>2</sub> Flux over the Global Ocean, *Deep-Sea Res. Pt. II*, 56, 554–577, 2009.
- Taylor, J. R. and Stocker, R.: Trade-Offs of Chemotactic Foraging in Turbulent Water, *Science*, 338, 675–679, 10.1126/science.1219417, 2012.
- Thompson, P. A., Wild-Allen, K., Lourey, M., Rousseaux, C., Waite, A. M., Feng, M., and Beckley, L. E.: Nutrients in an oligotrophic boundary current: Evidence of a new role for the Leeuwin Current, *Prog. Oceanogr.*, 91, 345–359, doi:10.1016/j.pcean.2011.02.011, 2011.
- Turner, J.: Buoyancy Effects in Fluids, Cambridge University Press, Cambridge, England, 367 pp., 1973.
- Valsala, V., Maksyutov, S., and Murtugudde, R.: A window for carbon uptake in the southern subtropical Indian Ocean, *Geophys. Res. Lett.*, 39, L17605, doi:10.1029/2012GL052857, 2012.
- Waite, A. M., Muhling, B. A., Holl, C. M., Beckley, L. E., Montoya, J. P., Strzelecki, J., Thompson, P. A., and Pesant, S.: Food web structure in two counter-rotating eddies based on  $\delta^{15}\text{N}$  and  $\delta^{13}\text{C}$  isotopic analyses, *Deep-Sea Res. Pt. II*, 54, 1055–

- 1075, doi:10.1016/j.dsr2.2006.12.010, 2007a.
- Waite, A. M., Thompson, P. A., Pesant, S., Feng, M., Beckley, L. E., Domingues, C. M., Gaughan, D., Hanson, C. E., Holl, C. M., Koslow, T., Meuleners, M., Montoya, J. P., Moore, T., Muhling, B. A., Paterson, H., Rennie, S., Strzelecki, J., and Twomey, L.: The Leeuwin Current and its eddies: An introductory overview, *Deep-Sea Res. Pt. II*, 54, 789–796, doi:10.1016/j.dsr2.2006.12.008, 2007b.
- Whitney, F. A., Freeland, H. J., and Robert, M.: Persistently declining oxygen levels in the interior waters of the eastern subarctic Pacific, *Progr. Oceanogr.*, 75, 179–199, 2007.
- Wijffels, S., Sprintall, J., Fieux, M., and Bray, N.: The JADE and WOCE I10/IR6 Throughflow sections in the southeast Indian Ocean. Part 1: water mass distribution and variability, *Deep-Sea Res. Pt. II*, 49, 1341–1362, doi:10.1016/s0967-0645(01)00155-2, 2002.
- Wolf-Gladrow, D. A., Zeebe, R. E., Klaas, C., Koertzing, A., and Dickson, A. G.: Total alkalinity: The explicit conservative expression and its application to biogeochemical processes, *Mar. Chem.*, 106, 287–300, 2007.
- Woo, M. and Pattiaratchi, C.: Hydrography and water masses off the western Australian coast, *Deep-Sea Res. Pt. I*, 55, 1090–1104, doi:10.1016/j.dsr.2008.05.005, 2008.
- Wyatt, A. S. J., Waite, A. M., and Humphries, S.: Variability in Isotope Discrimination Factors in Coral Reef Fishes: Implications for Diet and Food Web Reconstruction, *PLoS ONE*, 5, e13682, doi:10.1371/journal.pone.0013682, 2010.